Excitation mechanisms of the electron-beam-pumped atomic xenon ($5d \rightarrow 6p$) laser in Ar/Xe mixtures

Mieko Ohwa, Thomas J. Moratz,[a] and Mark J. Kushner[b]
University of Illinois, Department of Electrical and Computer Engineering, Gaseous Electronics Laboratory, 607 East Healey Street, Champaign, Illinois 61820

(Received 31 May 1989; accepted for publication 17 August 1989)

The atomic xenon laser operates on seven infrared transitions (1.73–3.51 μm) between the $5d$ and $6p$ manifolds. Intrinsic laser power efficiencies exceeding 5% have been previously obtained in Ar/Xe mixtures, principally at 1.73 μm ($5d[3/2]_1 \rightarrow 6p[5/2]_2$). The kinetic mechanisms responsible for this performance, though, are not well understood. In this paper, we report on a computer model for the electron-beam-pumped xenon laser in Ar/Xe mixtures with which we have investigated some of these excitation mechanisms. Based on the results of a parametric study of power deposition (50 W cm^{-3} to 100 kW cm^{-3}), gas pressure (0.5–6 atm), and xenon fraction, we suggest that the high efficiency obtained in Ar/Xe mixtures is due to rapid collisional cascade to the upper laser level of the 1.73-μm transition following dissociative recombination of $ArXe^+$ and selective quenching of the lower laser level of the 1.73-μm transition by collisions with argon. The results of our model indicate that the decrease in laser performance at high Xe fractions results from electron-impact excitation of the lower laser levels ($6s \rightarrow 6p$) and quenching of the $5d$ manifold by collisions with atomic xenon. The degradation of laser performance at high specific power deposition is most likely due to electron-collision mixing of the $5d$ and $6p$ manifolds. As a result of the lower levels being cleared dominantly by atomic collisions, we predict that optimum performance is then obtained at higher gas pressures when increasing power deposition. The results of the model predict that optimum power deposition is obtained when the fractional ionization is ≈ 2–3×10^{-6}.

I. INTRODUCTION

During the past few years, there has been a concerted effort to develop the atomic xenon laser as an efficient source of coherent radiation in the near infrared.[1–13] This laser is attractive from a system standpoint because its gas lifetime is expected to be long due to its use of only rare-gas mixtures. The xenon laser operates on seven infrared transitions (1.73–3.51 μm) between the $5d$ manifold (upper levels) and $6p$ manifold (lower levels). In specific gas mixtures, oscillation may also occur between the $7p$ and $7s$ manifolds at 3.43 and 3.65 μm. (See Table I and Fig. 1.) Intrinsic power efficiencies (laser power/pump power) of 3%–5% have thus far been demonstrated.[1,2,6,7,9] These high efficiencies have been obtained over a large parameter space in pump power (10's W cm^{-3} to 10's kW cm^{-3}), gas pressure (0.6–5 atm), and excitation method (e-beam, e-beam sustained discharge, and fission-fragment excitation). The laser operates efficiently over this large parameter space because the $6p$ manifold is depopulated by tight coupling to the $6s$ manifold by radiative transitions at low pressures ($<$ 100's Torr) and collisional quenching at high pressure. Inversions are therefore readily obtained by populating the $5d$ states.

Laser efficiency and the laser spectrum are sensitive functions of the gas mixture.[1] Ar/Xe, He/Xe, Ar/He/Xe, and Kr/Xe gas mixtures have been investigated by particle-beam excitation with xenon mole fractions of $< 10\%$.[2,9] The highest laser efficiencies have been obtained in Ar/Xe mixtures and Ar/He/Xe mixtures[9] with xenon mole fractions of 0.1%–2%. In Ar/Xe mixtures, the 1.73-μm transition carries $\geqslant 0.75$ of the power, while laser oscillation is quenched at Xe mole fractions in excess of 10%.

Since the most promising laser performance has been obtained in Ar/Xe mixtures, the majority of experimental work has been conducted on that system. In spite of this work, though, the excitation and quenching mechanisms that are responsible for the laser's performance are still topics of discussion. Early analysis of the laser's performance resulted in the hypothesis that dissociative recombination of $ArXe^+$ nearly directly populates the $5d$ manifold (upper laser level) of xenon, while dissociative recombination of Xe_2^+ leads directly to the $6p$ manifold (lower laser level).[3,13] These reaction pathways were used to explain why high laser efficiency is obtained in Ar/Xe mixtures, and why laser os-

TABLE I. Xe I infrared laser transitions.

Transition	Wavelength (μm)
$5d[3/2]_1 \rightarrow 6p[5/2]_2$	1.73
$\rightarrow 6p[3/2]_1$	2.03
$\rightarrow 6p[1/2]_0$	2.65
$5d[5/2]_3 \rightarrow 6p[5/2]_3$	2.48
$5d[5/2]_2 \rightarrow 6p[5/2]_2$	2.63
$\rightarrow 6p[3/2]_1$	3.37
$5d[7/2]_4 \rightarrow 6p[5/2]_2$	3.51
$7p[5/2]_2 \rightarrow 7s[3/2]_1$	3.43
$7p[1/2]_1 \rightarrow 7s[3/2]_2$	3.65

[a] Present address: Mission Research Corp., One Tara Blvd., Nashua, NH 03062.

[b] Author to whom correspondence should be addressed.

 0021-8979/89/235131-15$02.40

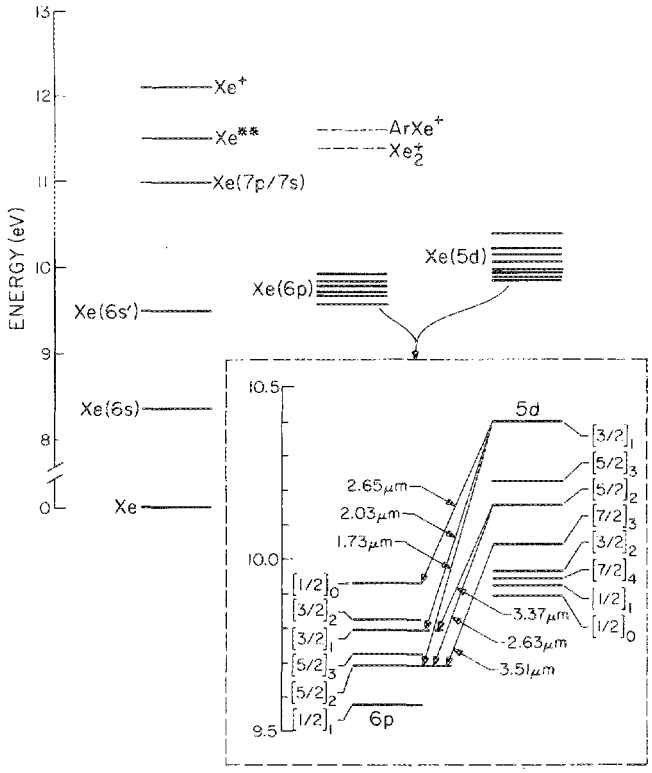

FIG. 1. Energies of the xenon levels included in the model. The positions of $ArXe^+$ and Xe_2^+ are shown for reference. The enlarged portion of the figure shows the xenon laser transitions.

cillation terminates at high xenon mole fractions. There is clear evidence, though, that other reaction pathways are also important in this respect. For example, laser oscillation on both $7p \rightarrow 7s$ and $5d \rightarrow 6p$ transitions has been obtained in the expansion phase of laser-produced plasmas in xenon where recombination is the dominant pumping mechanism.[12] These results indicate that recombination of Xe_2^+ may populate levels higher than the $6p$ manifold, enabling cascade excitation of the $5d$ manifold. The indirect, yet selective excitation of the upper laser level by recombination of $ArXe^+$ and Xe_2^+ is also suggested by the results of Peters, Mei, and Witteman.[5] They found that in e-beam-excited lasers the delay between the beginning of pumping to the onset of laser oscillation decreased with increasing gas pressure. From these results, they hypothesized that excitation of the $5d$ manifold is a consequence of atomic collision processes following recombination to higher excited states.

Further evidence of the more complex reaction mechanism can be found in the dependence of the laser spectrum on gas mixture. The 2.03- and 1.73-μm transitions share the same upper laser level ($5d[3/2]_1$), and the 2.03-μm transition has the higher oscillator strength. Therefore, one would expect that the 2.03-μm transition would dominate over the 1.73-μm transition under most conditions. This is, in fact, the case in He/Xe mixtures and in He/Ar/Xe mixtures having a large He mole fraction.[1-3,9] The 1.73-μm transition, however, dominates in Ar/Xe mixtures. This behavior implies that in Ar/Xe mixtures there must be some degree of selective quenching of the lower laser level of the 1.73-μm transition ($6p[5/2]_2$) by argon or that the 2.03-μm transition is suppressed by selective pumping of its lower laser level ($6p[3/2]_1$). These observations suggest that heavy-particle quenching reactions must be considered on a par with the pumping reactions to explain the laser's performance.

In this paper, we will use the results of a kinetics model to discuss the excitation mechanisms of the electron-beam-pumped atomic xenon laser operating in Ar/Xe gas mixtures. This discussion will include a survey of the gas pressures and power depositions which result in the maximum intrinsic laser power efficiency. The results of our model indicate that recombination of $ArXe^+$ is largely responsible for exciting the $5d$ manifold. The excitation process, though, is most likely indirect. Our model results are consistent with experiments when we specify that recombination is followed by heavy-particle quenching of higher excited states of xenon to both the $5d$ and $6p$ manifolds. We also find that the rate of recombination of Xe_2^+ is not sufficient to quench laser oscillation at high Xe mole fractions (2%–10%), and that there is experimental evidence suggesting that this recombination populates higher excited states. The quenching of laser oscillation at high xenon mole fraction appears to result dominantly from intramanifold quenching of the $5d$ levels by collisions with atomic xenon, with additional contributions from electron-impact excitation of the $6p$ manifold from the $6s$ levels and formation of xenon dimers which extract excitation from the atomic manifolds. By parametrizing the model and comparing to experiments, we propose that electron collisional mixing of the $6p$ and $5d$ manifolds is largely responsible for the increase in laser saturation intensity observed at increasing pump rates, and for the quenching of laser oscillation at high specific power deposition.

In Sec. II we review a selection of previous results from investigations of e-beam, discharge, and fission-fragment-pumped xenon lasers, and we discuss some implications of those results in Sec. III. In Sec. IV we describe our model for the xenon laser in Ar/Xe mixtures. Results from our model are discussed in Sec. V, followed by our concluding remarks in Sec. VI.

II. A REVIEW OF SELECTED PREVIOUS INVESTIGATIONS ON THE XENON LASER

In this section, we will briefly review selected previous experimental investigations of the atomic xenon laser. We will restrict our attention to studies of high-pressure ($\geqslant$0.5–1 atm) pulsed excitation by particle beams and discharges which relate to this work by providing information about the kinetic mechanisms responsible for the laser's performance.

Ar/Xe gas mixtures have thus far provided the basis of the most promising xenon lasers, and the majority of parametric studies have been performed on that system. Basov *et al.*[1-3] and Lawton *et al.*[13] investigated Ar/Xe mixtures at pressures above 1 atm, and first-order kinetic models of the laser were presented. Lawton *et al.*[13] investigated Ar/Xe mixtures excited by an e-beam sustained discharge. At a power deposition of 5–7 kW cm^{-3}, they obtained laser efficiencies of $>1\%$ with pulse lengths of 1–4 μs. With a xenon

mole fraction of 0.7% and gas pressure of 2.6 atm, the dominant laser transition was at 1.73 μm and the secondary transition was at 2.63 μm, carrying approximately 0.25 of the laser power. Due to there being ringing in the discharge circuit, power deposition varied during the excitation pulse which caused a variation in the laser spectrum as well. Higher power deposition favored the 1.73-μm transition, while lower power deposition favored the 2.63-μm transition.

Basov *et al.*[1] reported intrinsic energy efficiencies of 5% in an *e*-beam sustained discharge. They obtained intrinsic energy efficiencies $>1\%$–2% with *e*-beam pumping at a power deposition $\leqslant 70$ kW cm^{-3} and with a pulse duration of 3.5 μs. Maximum efficiency was obtained with xenon mole fractions of 0.5%–1.0% and at pressures of ≈ 3 atm.[2] At optimum conditions, the 1.73- and 2.63-μm transitions dominated, with the 1.73-μm transition carrying $\geqslant 0.90$ of the laser power. Basov *et al.*[1–3] found that above a xenon mole fraction of a few percent, the 1.73-μm transition quenched and the 2.63- and 2.65-μm transitions began to be dominant. At xenon mole fractions in excess of 10%, the 3.37-μm line is the dominant transition. At these higher mole fractions, though, total laser power decreased significantly, and so the absolute power obtained on transitions other than 1.73 μm is small.

The fact that intrinsic laser efficiencies in excess of 5% have been obtained in Ar/Xe mixtures is impressive considering that the quantum efficiency of the 1.73-μm transition (with respect to the ground state of xenon) is $\approx 7\%$. Lawton *et al.*[13] and Basov *et al.*[3] suggested that these high efficiencies are the result of there being a substantial amount of energy recirculating between the metastable state ($6s$) and the atomic ion. In this process, commonly called electroionization, laser oscillation occurs between the $5d$ and $6p$ manifolds, after which the $6p$ manifold relaxes to the metastable $6s$ (or $6s'$) states. The metastable states are then ionized by electron impact. After dimerization, cascading following recombination of $ArXe^+$ (or Xe_2^+) results in excitation of the $5d$ manifold. The quantum efficiency based on the electroionization cycle is $\approx 30\%$.

Recent investigations have been performed by Wexler *et al.*,[14] Suda *et al.*,[6,7] and Tucker *et al.*[15] at Naval Research Laboratory on *e*-beam, *e*-beam sustained-discharge, and self-sustained discharge excitation of Ar/Xe mixtures. With *e*-beam pumping, the power deposition was 7–42 kW cm^{-3} at gas pressures of 1–4 atm and pulse lengths of 2.5–3.0 μs. They obtained their highest intrinsic laser-energy efficiency of 2.6% at a xenon mole fraction of 0.5% at 3 atm, pumped at 24 kW cm^{-3}. With *e*-beam sustained-discharge excitation, the maximum intrinsic laser-energy efficiency was 3.2%. With self-sustained discharge-excitation there was poor coupling of the PFN to the discharge resulting from the low impedance of the plasma (0.05 Ω). The energy efficiency was therefore a low 0.4%. Approximately 75% of the laser power was at 1.73 μm and 20% at 2.63 μm at optimum conditions. At higher xenon mole fractions, the fractional laser power at 1.73 μm decreased with respect to that at 2.63 μm, while the fractional power at 2.65 μm increased significantly. The laser spectrum was only weakly dependent on total gas pressure between 2 and 4 atm.

Jacob[16] has also investigated *e*-beam-excited Ar/Xe mixtures. Their parameter space included a pressure range of 1.22–2.25 atm, power deposition of 2.2–16.2 kW cm^{-3}, and pulse length of 600 ns. At a xenon mole fraction of 0.5%, they obtained intrinsic laser efficiencies of 2.1%–3.9%. The laser power was dominantly at 1.73 μm due, in part, to optics which discriminated against the 2.6-μm transitions. With a gas pressure of 1.22 atm, they obtained a maximum in laser efficiency of 3.9% at a pump power of 6.8 kW cm^{-3}, decreasing to 2.1% at 16.2 kW cm^{-3}. By using a Rigrod analysis, Jacob estimated their small signal gain to be ≈ 0.06 cm^{-1} at 1.73 μm under optimum conditions. This high value would seem to confirm their observations of amplified spontaneous emission (ASE) as well as those by Suda *et al.*[6,7]

Particle-beam excitation of Ar/Xe mixtures at low-power deposition has been investigated by Alford and Hays[9] and Patterson, Samlin, and Brannon.[17] Alford and Hays investigated fission-fragment excitation of Ar/Xe and He/Ar/Xe mixtures at power deposition of 1–100 W cm^{-3} and pulse lengths of 200 μs to 5 ms. Using Ar/Xe mixtures the gas pressure was 0.6 atm with a xenon mole fraction of 0.5%. Intrinsic laser power efficiencies of 4.9%–5.8% were obtained at pumping powers of 2–10 W cm^{-3}. They observed, though, that laser oscillation could not be sustained for the entire pump pulse. Oscillation terminated after approximately 50 mJ cm^{-3} was deposited. Patterson and coworkers[17] investigated *e*-beam excitation of the same mixture at a power deposition of 0.1–1.0 kW cm^{-3}, gas pressure of 1.0 atm, and pulse length of 1 ms. They found that laser oscillation also terminated prematurely. The specific energy deposition at which oscillation terminated was found to be ≈ 200 mJ cm^{-3} for their range of pump powers.

Basov *et al.*[2] also investigated *e*-beam sustained-discharge pumping of He/Xe mixtures. With a gas mixture of 3.5 atm they observed that the dominant transition was at 2.03 μm. This transition shares the same upper laser level ($5d[3/2]_1$) as the 1.73-μm transition which dominates in Ar/Xe mixtures. The total laser power decreased to approximately 0.2 of that in Ar/Xe mixtures. Since the competing transitions share the same upper level, the differences in laser spectrum in the two mixtures must be attributed to differences in excitation or quenching of the $6p$ manifold. With helium as the buffer gas Basov *et al.*[2] obtained secondary transitions at 2.65 μm, and at 3.43 and 3.65 μm between the $7p$ and $7s$ manifolds. The latter transitions are not observed in Ar/Xe mixtures. Similar results were obtained by Peters and co-workers[4] using a coaxial electron beam, and by Lawton *et al.*[13] using an electron-beam sustained discharge. These results imply that recombination pumping in the He/Xe mixtures cascades through higher levels than in Ar/Xe mixtures. Alford and Hays[9] investigated fission-fragment excitation of He/Ar/Xe = 0.5/0.5/0.005 with a total pressure of 1.36 atm and power deposition of 4–500 W cm^{-3}. They obtained intrinsic laser efficiencies of 2.5%–3.3%, comparable to that obtained with Ar/Xe mixtures. The dominant transition in their mixture also changed from 1.73 to 2.03 μm when the helium mole fraction exceeded 0.2.

Basov *et al.*[2] also investigated Kr as a buffer gas and

obtained low efficiency compared to using argon as a buffer gas. The lasing transitions did not originate on the $5d[3/2]_1$ or $5d[5/2]_2$ levels as usually obtained when using argon and helium as buffer gases. Instead, the 3.51-μm ($5d[7/2]_3 \rightarrow 6p[5/2]_2$) and 2.48-$\mu$m ($5d[5/2]_3 \rightarrow 6p[5/2]_3$) transitions were the strongest. The 3.51-μm transition dominated with *e*-beam pumping; the 2.48-μm transition was competitive in the *e*-beam sustained discharge.

III. IMPLICATIONS OF PREVIOUS STUDIES

It has been generally observed that laser performance degrades with increasing partial xenon pressure above a mole fraction of a few percent. This observation has led to the suggestion that recombination of Xe_2^+ results in filling of the $6p$ manifold. However, in a plasma with >1 eV of available energy, recombination has been observed to populate all energetically accessible states.[18,19] The probability of filling the levels higher than the $6p$ levels is therefore highly probable, and experimental evidence discussed in the Introduction supports this observation. Dissociative recombination of Xe_2^+ is therefore not likely to be the sole cause for poor laser performance at high xenon mole fraction, and other processes may dominate. For example, the oscillator strengths for $6p \rightarrow 6s$ transitions are large. Therefore, electron-impact excitation from the heavily populated $6s$ states will likely be a major populating mechanism. Radiation trapping of the $6p \rightarrow 6s$ transitions at the higher xenon mole fractions could also contribute to a reduced rate of net relaxation of the $6p$ states. The decrease in laser power observed at large xenon mole fractions, though, merely implies that the density of the $6p$ lower laser levels increases at a higher rate than does the population of the $5d$ manifold. Therefore, the laser's performance could also be explained by an increased net rate of quenching of the $5d$ manifold.

In Ar/Xe mixtures, the 1.73-μm transition dominates with little, if any oscillation on the 2.03-μm transition, which has a larger oscillator strength. The fact that both transitions originate from the $5d[3/2]_1$ level indicates that the $6p[5/2]_2$ lower level of the 1.73-μm transition is quenched by argon collisions more quickly than the $6p[3/2]_1$ level (lower level for the 2.03-μm transition). The 1.73-μm transition also has a more favorable ratio of degeneracies than the 2.03-μm transition. Measurements of the rate constants for Ar quenching of $6p$ levels by Ku and Setser[20] showed that the $6p[5/2]_2$ level is rapidly quenched by argon, thereby partly explaining the dominance of the 1.73-μm transition. When the laser is operating at maximum efficiency, the $5d[3/2]_1$ is highly saturated, thereby contributing to the dominance of the 1.73-μm transition.

When the xenon fraction in an Ar/Xe mixture is increased to greater than a few percent, the fractional laser power at 1.73 μm decreases, or ceases, and the total laser power decreases. Coincidentally, the 2.63-μm transition becomes the dominant line, followed by the 2.65-μm transition.[1] The 1.73- and 2.65-μm transitions share the same upper laser level ($5d[3/2]_1$), while the 1.73- and 2.63-μm transitions share the same lower level ($6p[5/2]_2$). Oscillation on the 2.65-μm transition depopulates the $5d[3/2]_1$ upper level, which it shares with the 1.73-μm transition, while oscillation of the 2.63-μm transition fills the lower level of the 1.73-μm line. The combined effects quench the 1.73-μm transition. These results imply that when the mole fraction of Xe is increased, the net rate of excitation of the $5d[5/2]_1$, upper level of 2.63 μm, must increase compared to $5d[3/2]_1$, the upper level of the 1.73 μm. The change may be a combined effect of quenching of the upper level of the 1.73-μm transition and excitation of the upper level of the 2.63-μm transition. Analogously the net rate of excitation of $6p[5/2]_2$, lower level for 1.73 μm, must increase compared to $6p[1/2]_0$, lower level for 2.65 μm.

The importance of electron-collision processes (quenching and mixing of the $5d$ and $6p$ manifolds) is demonstrated by the combined results of many workers. Using a Rigrod analysis, Jacob,[16] Alford and Hays,[9] and Patterson and co-workers[17] have calculated the saturation intensity of 1.73 μm as a function of pump power from <10 W cm^{-3} to >10 kW cm^{-3}. Over this large range in pump power, the saturation intensity obeys I_s (W cm^{-2}) $\approx 12.9 P^{0.66}$, where P is the power deposition in W cm^{-3}.[17] Since the electron density in recombination dominated electron-beam-excited plasmas scales approximately as $P^{0.5}$, this scaling strongly suggests that the coherence time of the inversion is dominated by electron-collision processes.[6] The total lifetime of the inversion is also likely controlled by electron-collision processes, as suggested by the termination in laser output during a long excitation pulse when power deposition exceeded a critical value.[9]

IV. DESCRIPTION OF THE MODEL FOR ELECTRON-BEAM EXCITATION OF THE ATOMIC Xe LASER IN Ar/Xe MIXTURES

In this section we will describe our electron kinetics and plasma chemistry model for the electron-beam-excited atomic xenon laser. The framework of the model mechanically differs little from conventional models of excimer lasers using Ar and Xe, and we refer the reader to Refs. 21–23 for a listing of typical heavy-particle and electron-impact reactions. Our model does differ from those works in that we exclude the halogen and explicitly include the individual levels of the $6p$ and $5d$ manifolds of xenon in the reaction scheme in addition to the lumped states Xe($6s$), Xe($6s'$), and Xe($7p/7s$), and Xe** (higher radiating states). The additional levels included in our model are shown in Fig. 1.

A. Excitation mechanisms

In analyses of *e*-beam-pumped plasmas it is common to express the rate of excitation and ionization by beam electrons and their high-energy secondary electrons in terms of a W value (energy/event). In this manner, for example, the rate of ionization of a particular species is P/W, where P is the *e*-beam power deposition and W is the average energy expended to create an ion of that species. W values can be equivalently defined for excitation. It is well known that W values in mixtures do not simply scale from the W values of the pure gas components. We therefore calculated the W values for ionization and excitation of Ar and Xe, and the bulk electron temperature, for individual mixtures. These

TABLE II. Typical excitation parameters for e-beam pumping of Ar/Xe mixtures.

Process	W value (eV/event) Ar/Xe = 99.9/0.1	99.5/0.5	9/1
$e_b + Xe \rightarrow Xe(6s) + e_b$	1791	632	184.3
$e_b + Xe \rightarrow Xe(6p) + e_b$	4053	1351	208.4
$e_b + Xe \rightarrow Xe^+ + e_b + e$	6220	2480	109.9
$e_b + Ar \rightarrow Ar^* + e_b$	218.2	225.5	326.5
$e_b + Ar \rightarrow Ar^{**} + e_b$	58.6	59.1	72.4
$e_b + Ar \rightarrow Ar^+ + e_b + e$	28.9	29.2	35.4
Electron temperature (eV)	1.22	1.18	1.15

results were obtained with a Monte Carlo simulation for the slowing of high-energy beam electrons and their progeny. The model is described in detail in Ref. 24. Representative values for W values and electron temperatures appear in Table II. Excitation to the Xe($6p$) manifold was equally divided among the six levels.

In modifying the reaction scheme commonly used to describe excimer lasers, we treated the $6p$, $5d$, and $7p/7s$ manifolds in our model equivalently to Xe** in terms of the possible electron-impact and heavy-particle reactions if we had no state-selective information. Unless stated differently, we also used the same rate constants. For example, we included the dimer association reaction

$$Xe^{**} + Ar + Ar \rightarrow ArXe^* + Ar, \qquad (1)$$

for all $6p$, $5d$, and $7p/7s$ levels in the model using the same rate constant as for Xe**. The differences in excitation and quenching of individual levels in the $6p$ and $5d$ manifolds, though, are the important processes in describing the laser performance. There are obviously many processes that can lead to populating the $5d$ and $6p$ levels of the atomic xenon laser. In Ar/Xe mixtures, in addition to direct electron-impact excitation from the ground-state, dissociative recombination of Xe_2^+ and $ArXe^+$, energy transfer from Ar* and Ar_2^*, electron-impact mixing between excited states, and heavy-particle quenching of higher excited states may result in excitation of the $5d$ and $6p$ manifolds. Electron-impact and heavy-particle processes, and their rate constants, which involve excited states of Xe used in the model, are listed in Table III. Some of the more important processes are discussed below.

The Xe levels directly populated by dissociative recombination of Xe_2^+ have been studied by Shiu *et al.*[18,19] Those investigations were not intended to be a detailed study of the exit channels, as they observed a limited range of the radiative cascades. They concluded that the only constraint on the state of excited xenon atoms resulting from dissociative recombination is the available energy in the plasma and the energy of the final state. By analogy, a similar argument can be made for the states directly populated by the dissociative recombination of $ArXe^+$.[6] With these observations, we initially allowed that recombination of $ArXe^+$ and Xe_2^+ populate all levels above and including Xe($6s$), with the former dominantly populating Xe** and Xe ($7p/7s$), and the latter dominantly populating Xe($6s'$). The redistribution of population from the Xe** and Xe ($7p/7s$) states to the $5d$ and $6p$ manifolds then occurs by radiative relaxation, and heavy-particle and electron collisions. The final branching to individual levels in the $5d$ and $6p$ manifolds were obtained by parametrizing the model and comparing to experimental data. The criteria we used in obtaining these branching ratios is that we must reproduce the experimental dependence of total laser power on Xe mole fraction ($\leqslant 10\%$), total laser power on gas pressure, and the laser spectrum as a function of gas mixture. Experimental data from Basov *et al.*,[1] Suda *et al.*,[6,7] and Wexler *et al.*[14] were used for this purpose. The branching ratios so derived are listed in Table IV. These branchings are not unique as other combinations of branching ratios and values of rate constants may also reproduce experimental results. We feel, though, that these values reflect the pertinent physical processes responsible for laser performance.

Energy transfer from Ar* to excited states of xenon was also included in the model. The total rate coefficient for energy exchange to all Xe levels from $Ar^*(^3P_2, ^3P_0)$ is 2.1×10^{-10} cm^3 s^{-1}.[27] The Xe levels having the highest probability for excitation are those which are resonant. King, Piper, and Setser[38] studied the states of xenon produced in this reaction and found that the dominant products were Xe($7d$) and Xe($8d$), with the $7d$ manifold accounting for half of the excitation. The only other sizeable contributions were to Xe($5f$) and Xe ($6f$). We therefore assign all excitation transfer from Ar* to Xe**. In a similar fashion, we assigned excitation transfer from Ar_2^* to Xe($6s'$).[39]

B. Thermal electron-collision processes

Electron-impact excitation from the $6s$ to the $6p$ manifold, and electron-collision mixing between the $6p$ and $5d$ manifolds are largely responsible for the dependence of laser power on gas mixture and power deposition, in addition to heavy-particle quenching of the $5d$ and $6p$ manifolds. Relative contributions to the quenching of the $5d$ and $6p$ manifolds by electron collisions and heavy-particle processes are determined by the fractional ionization. Electron-impact cross sections for excitation between individual levels of the Xe($6s$), $6p$, $5d$, and $7p/7s$ manifolds are not well known. Estimates of the temperature-dependent rate constant for electron-impact excitation of Xe($6s$) to higher-lying levels are available.[40] Since the oscillator strength for transitions between $6s$ and $6p$ levels are large, while transitions between the $6s$ and $5d$ manifolds are forbidden, one would except a higher rate of mixing by electron impact between the $6s$ and $6p$ manifolds. Based on this logic, we apportioned the rate constant for total excitation out of Xe($6s$) and to the $6s'$ and $6p$ manifolds, assuming that the excitation is dominantly out of the $6s[3/2]_2$ level. To account for the differences between allowed and forbidden transitions, excitation collisions to the $6p$ manifold were weighted by their oscillator strengths and transitions to the $5d$ manifold were not allowed. The weighting of electron-impact excitation rates by their oscillator strengths must be considered only an approximation, since optically forbidden transitions can have large cross sections near threshold. Additionally, the rate constants were

TABLE III. Reactions and rate coefficients involving Xe excited states used in the model for the atomic Xe laser in Ar/Xe mixtures.

Process[a]		
Electron-impact processes	Rate coefficient[b]	Reference
$Xe(6s) + e \rightleftarrows Xe(6p) + e$	c	d
$Xe(6s) + e \rightleftarrows Xe(7p,7s) + e$	$2.75(-7)\,T_e^{0.8}\exp\left(\frac{-2.68}{T_e}\right)$	c,d
$Xe(6s) + e \rightleftarrows Xe^{**} + e$	$2.75(-7)\,T_e^{0.8}\exp\left(\frac{-3.18}{T_e}\right)$	c,d
$Xe(6s') + e \rightleftarrows Xe(6p[1/2]_1) + e$	$5.0(-8)\,T_e^{0.8}$	c,d
$Xe(6s') + e \rightleftarrows Xe(7p,7s) + e$	$1.0(-7)\,T_e^{0.8}\exp\left(\frac{-1.5}{T_e}\right)$	c,d
$Xe(6s') + e \rightleftarrows Xe^{**} + e$	$5.5(-7)\,T_e^{0.8}\exp\left(\frac{-2.0}{T_e}\right)$	c,d
$Xe(7p,7s) + e \rightleftarrows Xe^{**} + e$	$1.0(-7)\,T_e^{0.8}\exp\left(\frac{-1.0}{T_e}\right)$	c,d
$Xe^* + e \rightarrow Xe^+ + e + e$	c	
$Xe(5d_j) + e \rightleftarrows Xe(5d_k) + e$	c	d
$Xe(6p_j) + e \rightleftarrows Xe(6p_k) + e$	c	d
$Xe(6p_j) + e \rightleftarrows Xe(5d_k) + e$	c	d
$Xe_2^+ + e \rightarrow Xe^* + Xe$	$8.2(-7)\left[1-\exp\left(\frac{-180}{T_g}\right)\right]T_e^{-1/2}$	25,26,e
$ArXe^+ + e \rightarrow Xe^* + Ar$	$3.5(-7)\left[1-\exp\left(\frac{-180}{T_g}\right)\right]T_e^{-1/2}$	25,26,e
Heavy particle processes		
$Ar^* + Xe \rightarrow Xe^{**} + Ar$	$2.10(-10)$	27
$Xe^* + Ar + Ar \rightleftarrows ArXe^* + Ar$	$1.00(-33)$	28,f
$Ar^* + Xe + Ar \rightleftarrows XeAr^* + Ar$	$1.00(-33)$	28,f,g
$ArXe^* + Xe \rightarrow Xe_2^* + Ar$	$1.00(-10)$	29
$Ar_2^* + Xe \rightarrow Ar + Ar + Xe(6s')$	$4.39(-10)$	30
$Xe^{**} + M \rightarrow Xe(6s) + M$	$M = Xe, 3.00(-10); M = Ar, 1.00(-10)$	31
$Xe^{**} + M \rightarrow Xe(7p,7s) + M$	$M = Xe, 5.00(-11); M = Ar, 1.00(-11)$	estimate
$Xe(7p,7s) + M \rightarrow Xe^* + M$	$M = Xe, 1.00(-10); M = Ar, 1.00(-11)$	e,h
$Xe(6s) + Xe(6s) \rightarrow Xe^+ + Xe + e$	$5.00(-10)$	32
$Xe(6s) + Xe + M \rightarrow Xe_2^* + M$	$M = Xe, 5.00(-32); M = Ar, 2.50(-32)$	33,i
$Xe(5d[1/2]_0) + Xe + M \rightarrow Xe(6s) + Xe + M$	$M = Xe, 5.00(-32); M = Ar, 2.50(-32)$	33,i
$Xe(5d[1/2]_1) + Xe + M \rightarrow Xe(6s) + Xe + M$	$M = Xe, 5.00(-32); M = Ar, 2.50(-32)$	33,i
$Xe(5d[7/2]_4) + Xe + M \rightarrow Xe(6s) + Xe + M$	$M = Xe, 5.00(-32); M = Ar, 2.50(-32)$	33,i
$Xe(5d[3/2]_2) + Xe + M \rightarrow Xe(6s) + Xe + M$	$M = Xe, 5.00(-32); M = Ar, 2.50(-32)$	33,i
$Xe(5d[7/2]_3) + Xe + M \rightarrow Xe(6s) + Xe + M$	$M = Xe, 5.00(-32); M = Ar, 2.50(-32)$	33,i
$Xe(5d[5/2]_2) + Xe + M \rightarrow Xe(6p[5/2]_2) + Xe + M$	$M = Xe, 5.00(-32); M = Ar, 2.50(-32)$	33,i
$Xe(5d[5/2]_3) + Xe + M \rightarrow Xe(6p[5/2]_2) + Xe + M$	$M = Xe, 5.00(-32); M = Ar, 2.50(-32)$	33,i
$Xe(5d[3/2]_1) + Xe + M \rightarrow Xe(6p[5/2]_2) + Xe + M$	$M = Xe, 5.00(-32); M = Ar, 2.50(-32)$	33,i
$Xe(7p,7s) + Xe + M \rightarrow Xe(6s') + Xe + M$	$M = Xe, 5.00(-32); M = Ar, 2.50(-32)$	33,i
$Xe^{**} + Xe + M \rightarrow Xe(6s') + Xe + M$	$M = Xe, 5.00(-32); M = Ar, 2.50(-32)$	33,i
$Xe(6s') + Xe + M \rightarrow Xe_2^* + M$	$M = Xe, 5.00(-32); M = Ar, 2.50(-32)$	33,i
$Xe(6p) + Xe + M \rightarrow Xe_2^* + M$	$M = Xe, 5.00(-32); M = Ar, 2.50(-32)$	33,i
$Xe(6p[1/2]_0) + Xe + M \rightarrow Xe_2^* + M$	$M = Xe, 6.57(-31); M = Ar, 3.29(-31)$	33,i
$Xe(5d[1/2]_1) + M \rightarrow Xe(6p[1/2]_0) + M$	$M = Xe, 9.50(-11); M = Ar, 3.80(-11)$	20
$Xe(6p[1/2]_0) + Ar \rightarrow Xe(6p[3/2]_2) + Ar$	$4.00(-11)$	20
$\rightarrow Xe(5d[1/2]_1) + Ar$	$1.00(-10)$	20
$Xe(6p[1/2]_0) + Xe \rightarrow Xe(6p[3/2]_2) + Xe$	$1.33(-12)$	20
$\rightarrow Xe(6p[3/2]_1) + Xe$	$0.87(-12)$	20
$\rightarrow Xe(6p[5/2]_3) + Xe$	$1.58(-12)$	20
$\rightarrow Xe(6p[5/2]_2) + Xe$	$1.29(-12)$	20
$\rightarrow Xe(6s') + Xe$	$0.90(-12)$	20
$Xe(6p[3/2]_2) + M \rightarrow Xe(6s') + M$	$M = Xe, 1.90(-11); M = Ar, 1.09(-11)$	20,34
$\rightarrow Xe(6p[3/2]_1) + M$	$M = Xe, 1.30(-11); M = Ar, 7.45(-12)$	20,34
$\rightarrow Xe(6p[5/2]_3) + M$	$M = Xe, 2.10(-11); M = Ar, 1.2(-11)$	20,34
$\rightarrow Xe(6p[5/2]_2) + M$	$M = Xe, 2.80(-11); M = Ar, 1.6(-11)$	20,34
$\rightarrow Xe(6p[1/2]_1) + M$	$M = Xe, 1.00(-12); M = Ar, 5.73(-13)$	20,34
$Xe(6p[3/2]_1) + M \rightarrow Xe(6s') + M$	$M = Xe, 1.24(-10); M = Ar, 1.31(-11)$	35,j
$\rightarrow Xe(6p[3/2]_2) + M$	$M = Xe, 1.20(-11); M = Ar, 1.28(-12)$	35,j
$\rightarrow Xe(6p[5/2]_3) + M$	$M = Xe, 1.20(-10); M = Ar, 1.28(-11)$	35,j
$Xe(6p[5/2]_3) + M \rightarrow Xe(6s') + M$	$M = Xe, 1.80(-11); M = Ar, 6.79(-12)$	20,34
$\rightarrow Xe(6p[5/2]_2) + M$	$M = Xe, 3.10(-11); M = Ar, 1.17(-11)$	20,34
$\rightarrow Xe(6p[1/2]_1) + M$	$M = Xe, 4.00(-12); M = Ar, 1.51(-12)$	20,34
$Xe(6p[5/2]_2) + M \rightarrow Xe(6s') + M$	$M = Xe. 1.80(-10); M = Ar, 2.08(-11)$	35,j
$\rightarrow Xe(6p[5/2]_3) + M$	$M = Xe, 4.95(-11); M = Ar, 5.80(-12)$	35,j
$\rightarrow Xe(6p[1/2]_1) + M$	$M = Xe, 2.03(-10); M = Ar, 2.34(-11)$	35,j

TABLE III (*continued*).

Process[a] Electron-impact processes	Rate coefficient[b]	Reference
$Xe(6p[1/2]_1) + M \rightarrow Xe(6s') + M$	M = Xe, 1.33(− 10); M = Ar, 3.00(− 12)	35,36
$Xe(6s') + M \rightarrow Xe(6p[1/2]_1) + M$	M = Xe, 6.70(− 11); M = Ar, 2.10(− 13)	35,36
$Xe(6s') + M \rightarrow Xe(6s) + M$	1.00(− 13), M = Ar, Xe	est.,36
$Xe(6s') + Xe \rightarrow Xe + Xe$	3.50(− 15)	estimate
$Xe(6s) + Xe \rightarrow Xe + Xe$	3.50(− 15)	estimate
$Xe(5d[3/2]_1) + Xe \rightleftarrows Xe(5d[5/2]_3) + Xe$	3.00(− 10)	f,j
$Xe(5d[5/2]_1) + Xe \rightleftarrows Xe(5d[5/2]_2) + Xe$	3.00(− 10)	f,j
$Xe(5d[5/2]_2) + Xe \rightleftarrows Xe(5d[7/2]_3) + Xe$	2.00(− 10)	f,j
$Xe(5d[7/2]_3) + Xe \rightleftarrows Xe(5d[3/2]_2) + Xe$	1.00(− 11)	f,j
$Xe(5d[3/2]_2) + Xe \rightleftarrows Xe(5d[7/2]_4) + Xe$	1.00(− 11)	f,i
$Xe(5d[7/2]_4) + Xe \rightleftarrows Xe(5d[1/2]_1) + Xe$	1.00(− 11)	f,i
$Xe(5d[1/2]_1) + Xe \rightleftarrows Xe(5d[1/2]_0) + Xe$	1.00(− 11)	f,i
$Xe(5d_i) + Ar \rightleftarrows Xe(5d_j) + Ar$	1.00(− 12)	f,i
Radiative transitions		
$Xe^{**} \rightarrow Xe(6s)$	6.00(6)	28
$Xe(7p,7s) \rightarrow Xe(6s)$	4.64(6)	37,k
$Xe(5d[5/2]_3) \rightarrow Xe(6s)$	4.25(5)	37,k
$Xe(5d[5/2]_2) \rightarrow Xe(6s)$	3.94(5)	37,k
$Xe(5d[7/2]_3) \rightarrow Xe(6s)$	1.07(5)	37,k
$Xe(6p[1/2]_0) \rightarrow Xe(6s)$	3.07(7)	20,k
$Xe(6p[3/2]_2) \rightarrow Xe(6s)$	2.78(7)	20,k
$Xe(6p[3/2]_1) \rightarrow Xe(6s)$	2.72(7)	20,k
$Xe(6p[5/2]_3) \rightarrow Xe(6s)$	3.10(7)	20,k
$Xe(6p[5/2]_2) \rightarrow Xe(6s)$	2.54(7)	20,k
$Xe(6p[1/2]_1) \rightarrow Xe(6s)$	2.62(7)	20,k
$Xe(7p,7s) \rightarrow Xe(6s')$	2.89(6)	28,37
$Xe(5d[1/2]_0) \rightarrow Xe(6p[1/2]_1)$	2.33(5)	28,37
$Xe(5d[1/2]_1) \rightarrow Xe$	1.12(7)	31
$Xe(5d[7/2]_4) \rightarrow Xe(6p[5/2]_3)$	1.90(5)	31
$Xe(5d[3/2]_2) \rightarrow Xe(6p[1/2]_1)$	4.00(5)	31
$Xe(5d[7/2]_3) \rightarrow Xe(6p[5/2]_2)$	7.33(5)	31
$Xe(5d[5/2]_3) \rightarrow Xe(6p[3/2]_2)$	1.39(6)	31
$Xe(5d[3/2]_1) \rightarrow Xe$	1.67(9)	31,k
$Xe(5d[3/2]_1) \rightarrow Xe(6p[5/2]_2)$	3.04(5)	37
$Xe(5d[3/2]_1) \rightarrow Xe(6p[3/2]_1)$	2.46(6)	37
$Xe(5d[5/2]_2) \rightarrow Xe(6p[5/2]_2)$	7.42(5)	37
$Xe(5d[3/2]_1) \rightarrow Xe(6p[1/2]_0)$	1.27(6)	37
$Xe(5d[5/2]_2) \rightarrow Xe(6p[3/2]_1)$	6.81(5)	37

[a] Xe* denotes any excited state of Xe. Xe(6*p*) or Xe(5*d*) denotes any level in that manifold.
[b] 1.4(− 10) = 1.4×10^{-10}. Coefficients have units of s^{-1}, $cm^3\ s^{-1}$, and $cm^6\ s^{-1}$ for first-, second-, and third-order reactions, respectively. The electron temperature T_e has units eV; and gas temperature T_g has units K. See Sec. IV F for other gas-temperature dependencies.
[c] See text, Sec. IV B.
[d] Reverse reaction is by detailed balance based on the electron temperature.
[e] For branching to excited states of Xe, see Table IV.
[f] Reverse reaction is by detailed balance based on the gas temperature.
[g] In analogy to Xe* + 2Ar → ArXe* + Ar.
[h] See text, Sec. IV A.
[i] See text, Sec. IV C.
[j] See text, Secs. IV and V.
[k] Radiation trapping factors included. See text, Sec. IV D.

weighted by their Boltzmann factors. Using the form of the rate constant or $6s \rightarrow 6p$ excitation from Ref. 40, the rate constants we used for $6s \rightarrow 6p$ are

$$k(6p_i) = f_i 9.2\times10^{-7} T_e^{0.79} \exp(-u_i/T_e)\ \text{cm}^3\ \text{s}^{-1}, \quad (2)$$

where u_i is the excitation potential relative to the $6s[3/2]_2$ and f_i is the transition probability relative to the $6p[1/2]_1$ level. The rates of electron-collision quenching from these levels to Xe(6*s*) are obtained by detailed balance.

Since the optical transitions between levels in 6*p* and 5*d* manifolds have high oscillator strengths, one might expect that these manifolds are also tightly coupled by electron-collision mixing. As we will discuss below, electron-collision mixing of the 6*p* and 5*d* manifolds may be primarily responsible for terminating the laser at high specific power depo-

TABLE IV. Branching ratios for Xe excitation reactions.

Reaction	Product Xe* level	Branching ratio
$e + Xe_2^+ \rightarrow Xe + Xe^*$	$(7p,7s)$	0.1
	$6p[1/2]_1$	0.45
	$6s'$	0.45
$e + ArXe^+ \rightarrow Ar + Xe^*$	Xe**	0.1
	$(7p,7s)$	0.9
$Xe(7p,7s) + Xe \rightarrow Xe + Xe^*$	$5d[5/2]_2$	0.5
	$6p[3/2]_1$	0.2
	$6p[5/2]_2$	0.3
$Xe(7p,7s) + Ar \rightarrow Ar + Xe^*$	$5d[3/2]_1$	0.7
	$6p[3/2]_1$	0.2
	$6p[1/2]_0$	0.1

sition. To account for this electron-collision mixing, we included the processes $e + Xe(6p_i) \rightleftarrows Xe(5d_i) + e$ between all levels of the $6p$ and $5d$ manifolds. Lacking theoretical or experimental information on the cross sections, all exothermic processes were assigned the same rate constant of 2×10^{-7} cm^3 s^{-1}, which was determined by parametrizing the model and comparing to experiment. The rate constants for the reverse processes were obtained by detailed balance

$$k_{ij} = k_{ji}\left(\frac{g_j}{g_i}\right)\exp\left(-\frac{(u_i - u_j)}{kT_e}\right), \tag{3}$$

where g_i and u_i are the degeneracies and energy of level i. Ionization out of all excited states was included by using the rate constant $[(1.1\times10^{-6})/\Delta\epsilon^2]T_e^{0.7}\exp(-\Delta\epsilon/T_e)$ cm^3 s^{-1}, where $\Delta\epsilon$ is the ionization potential (eV) of the state.[40]

Electron-collision mixing within a particular manifold ($6p$ or $5d$) results in thermalizing of the manifold to a distribution characterized by the electron temperature T_e. We included this process by estimating the rate constant for thermalization, which was then included in the rate equations for each level. The rate for thermalization was approximated by

$$\frac{\partial[Xe_i]}{\partial t} = \frac{[Xe_i] - [Xe_i]_0}{\tau_e}, \quad \tau_e^{-1} = k_e(T_e)n_e, \tag{4}$$

where the thermal equilibrium value is

$$[Xe_i]_0 = \sum_j [Xe_j]\frac{g_i\exp(-u_i/T_e)}{\Sigma_j g_j\exp(-u_j/T_e)}. \tag{5}$$

$[Xe_i]$ is the density of level i in a particular manifold, u_i is its energy relative to the lowest level of the manifold, $k_e(T_e)$ is the rate constant for electron collisions, n_e is the electron density, and τ_e is the equilibrium time by electron collisions. We estimated that $k_e(T_e)$ is the same as that for electron-momentum transfer collisions. Since the spacing between levels is $\lesssim 0.1$ eV and the average electron energy is > 1–2 eV, virtually all electrons may contribute to mixing.

C. Heavy-particle quenching of the Xe(6p) and Xe(5d) manifolds

Quenching of levels in the Xe($6p$) and Xe($5d$) manifolds by heavy particles (i.e., Ar and Xe) is dominantly responsible for the change in the laser spectrum as a function of gas mixture. Selective quenching of individual levels of the $5d$ and $6p$ manifolds enable oscillation to dominantly occur on laser transitions which are either not directly strongly pumped or which are in competition with transitions from the same upper laser level which have higher oscillator strengths.

Experimentally derived rate constants are available for a subset of these processes. Rate constants for quenching of Xe($6p$) levels by xenon atoms have been measured by Ku and Setser,[20] Bowering, Bruce, and Keto,[35] Horiguchi, Chang, and Setser[34] and Inoue, Ku, and Setser.[36] Those rates were used and listed in Table III unless noted otherwise. Quenching of Xe($6p$) by argon is also fairly well understood. Here, though, there are notable exceptions to the analogous quenching reactions by xenon. For quenching of the Xe($6p[1/2]_0$) level by argon, we used the mechanisms suggested by Ku and Setser.[20] This mechanism includes mixing between the $6p[1/2]_0$ and $5d[1/2]_1$ levels, with the exchange favoring the exothermic transfer from $6p[1/2]_0$ to $5d[1/2]_1$. The quenching rates of the $6p[3/2]_2$ and $6p[5/2]_3$ levels by argon were based on those of Horiguchi and co-workers.[34] The rate constant for quenching of $6p[5/2]_2$ by argon is large compared to that of $6p[3/2]_1$. The rate constants we used for the former process are based on Ku and Setser,[20] and were defined by comparing the calculated laser spectrum with experiment over a large parameter space of pressure and gas mixture. The rate constants for the latter were obtained in the same fashion based on Horiguchi and co-workers.[34] The branchings for these quenching reactions were assumed to be the same as for quenching by xenon unless specific experimental results were available. The larger rate of quenching of the lower laser level of the 1.73-μm transition compared to the 2.03-μm transition by argon is partly responsible for that transition dominating in Ar/Xe mixtures. The branching for quenching of $6p[1/2]_1$ by argon is that given by Ku and Setser.[20]

Quenching of the $6p$ and $5d$ manifolds of xenon may also occur by three-body collisions. Analysis of the molecular potentials and curve crossing for Xe_2 suggests that three-body collisions of Xe atoms in the $5d$ manifold with ground-state Xe do not result in dimerization, but predissociate to Xe($6s$).[35] A similar process is likely to occur for the higher levels of Xe($6p$), while the lower levels of Xe($6p$), Xe($6p'$), and Xe($6s$) most likely dimerize. With these considerations, the branching for these quenching and association reactions are listed in Table III.

There is very little known about the quenching of the Xe($5d$) manifold by heavy particles. As a result, we estimated that heavy-particle collisions of Xe($5d$) levels by Ar are generally not selective and result in thermalization of the

manifold to the gas temperature. The rate of thermalization was estimated in the same manner as for electrons [see Eqs. (4) and (5)] where the gas temperature T_g is substituted for T_e. The rate constant for heavy-particle collisions was estimated to be 1.0×10^{-12} cm^3 s^{-1} for argon.

With increasing xenon mole fractions in Ar/Xe mixtures, the dominant laser transition changes from 1.73 to 2.63 μm. Since these transitions share the same lower level, these results imply that the upper level of the 1.73-μm transition preferentially quenched, or the upper level of the 2.63-μm transition is preferentially excited with increasing xenon mole fraction. In parametrizing the model as a function of gas mixture, we found that only quenching by Xe atoms could have a high enough rate with increasing xenon fraction to account for these processes. We therefore hypothesized that quenching (by atomic Xe) of $Xe(5d[3/2]_1) \rightarrow Xe(5d[5/2]_3)$ and $Xe(5d[5/2]_3) \rightarrow Xe(5d[5/2]_2)$ occurs with rate constant 3×10^{-10} cm^3 s^{-1}, while that for $Xe(5d[5/2]_2) \rightarrow Xe(5d[7/2]_3)$ proceeds with rate constant 2×10^{-10} cm^3 s^{-1}. These values have the effect of quenching laser oscillation at high xenon fraction with slight bottlenecking on $5d[5/2]_2$ which favors oscillation on the 2.63-μm transition over the 1.73-μm transition. This quenching is discussed further in Sec. V A.

D. Radiation trapping

Many of the lower laser levels in the $6p$ manifold have sufficiently short radiative lifetimes ($\lesssim$10's ns) that at low partial pressures of xenon radiative decay of the lower laser levels is sufficient to clear those levels during laser oscillation. At xenon pressures and pump rates that result in the density of Xe($6s$) exceeding 10^{14} cm^{-3}, these transitions may become radiatively trapped. Clearing of the lower laser levels must then proceed by collisional processes. The opposite effect results from radiation trapping of the upper laser levels. The short resonant radiative lifetime of $Xe(5d[3/2]_1)$ (<1 ns) works against efficient laser oscillation by increasing the saturation intensity and threshold pumping rate for laser transitions out of that level. At xenon partial pressures exceeding a few hundred mTorr, resonance radiation from $Xe(5d[3/2]_1)$ is trapped to the degree that other quenching processes dominate. Under these conditions, laser oscillation is observed from that level. In low-pressure xenon lasers where the $Xe(5d[3/2]_1)$ is not totally trapped and rapidly radiatively decays, transitions from $Xe(5d[3/2]_1)$ are not observed. To account for the effects of radiation trapping, the radiative lifetimes of $6p\rightarrow6s$ transitions, and that for resonance radiation from the $Xe(5d[3/2]_1)$, were lengthened according to the trapping factors described by Holstein[41] using transverse dimensions of a few cm. For these dimensions, typical of the devices we are simulating, trapping of the $5d[3/2]_1$ is important. Typically, trapping of the $6p\rightarrow6s$ transitions is not important.

E. Gain model

We explicitly included laser fluxes for transitions at 1.73, 2.63, 2.65, 3.37, and 2.03 μm. The gain model assumes that all transitions are collisionally broadened having Lorentzian line shapes. Collisional broadening occurs by both heavy-particle and electron collisions. For heavy particles the rate constant for collisional broadening is the larger of 5×10^{-11} cm^3 s^{-1} and the sum of other quenching collisions. A large contribution from electron collisional broadening is indicated from measurements of saturation intensity as a function pump power. We attribute the large value to both low-energy dephasing collisions and quenching collisions. The empirically derived rate coefficient for electron dephasing collisions is 5×10^{-6} cm^3 s^{-1}.

F. Gas-temperature dependence

The dependence of rate coefficients on gas temperature is the same as described in Ref. 43. The effects of high-energy loading, and high gas temperature, on xenon laser performance will be described in an upcoming publication.

V. PARAMETRIC STUDY OF THE PERFORMANCE OF THE Xe LASER

In this section we will discuss intrinsic efficiency (laser power/power deposition) of the atomic xenon laser in Ar/Xe mixtures as a function of xenon mole fraction, gas pressure, and power deposition. The optimum operating conditions will be discussed using the quasi-steady-state intrinsic power efficiency as a measure of performance. Previous experimental results have shown that the laser performance is a complex function of the pumping conditions. This complexity dominantly results from two causes. First, the laser spectrum and intrinsic power efficiency are functions of time during the pumping pulse. Although the dominant laser transition in the quasi steady state is usually at 1.73 μm, other transitions may transiently oscillate during the rising edge of the current pulse. Therefore, the fact that a particular transition in the steady state yields negligible power does not preclude its oscillation earlier during the pulse. The second cause for complexity is that the laser spectrum is a sensitive function of gas mixture. Therefore, observations made of laser performance in a single gas mixture are not necessarily indicative of typical, or optimum, laser performance. For example, one indication of operating with near optimum conditions in Ar/Xe mixtures is that the 1.73-μm transition carries most of the laser power; oscillation of 2.03 μm indicates that the pump rate is less than optimum. In the following section we will examine laser performance over a fairly large parameter space to investigate some of these issues.

A. Dependence of laser performance on xenon fraction

The experimental results of Basov *et al.*,[1-3] Suda *et al.*,[6] and Wexler *et al.*[14] for gas pressures of 3–4 atm and power deposition of >10 kW cm^{-3} have shown that laser efficiency and the laser spectrum in Ar/Xe mixtures are strongly dependent on the xenon fraction. Laser efficiency was found to increase with increasing Xe mole fraction up to a value of 0.1%–2%, after which efficiency decreased. These results have also shown that the laser efficiency is strongly correlated with the laser power obtained on the 1.73-μm transition. According to the results of this model, at xenon fractions greater than the optimum value, the intensity of the 1.73-μm transition decreases in spite of an increase in the

rate of population for its upper laser level ($5d[3/2]_1$). The observed decrease in laser efficiency and in the intensity of the 1.73-μm transition must then be attributed to either an increase in the population of its lower level ($6p[5/2]_2$) or an increase in the rate of quenching of $5d[3/2]_1$. Experimental results show, however, that all of the laser transitions which share the same upper level as the 1.73-μm transition decrease in intensity above the optimum xenon fraction. This observation strongly suggests that laser efficiency decreases at high xenon fraction due to an increase in the rate of quenching of the $5d[3/2]_1$ level. This suggestion is further reinforced by the fact that the lower laser level of the 1.73-μm transition, $6p[5/2]_2$, has a large degeneracy which reduces its relative importance in terminating laser oscillation.

To investigate these issues we parametrized the model for various xenon fractions and compared the results with experimental data. We first investigated the possibility that the decrease in laser intensity at high xenon fraction may be a result of population of the $6p$ manifold by dissociative recombination of Xe_2^+, as suggested by previous investigators, or by electron-impact excitation from the $6s$ levels. We parametrized the branching ratios for dissociative recombination of Xe_2^+, primarily to the $6s$, $6s'$, and $6p$ manifolds, and found that the rate of excitation of the $6p$ manifold by this process is not large enough to quench laser oscillation as observed experimentally. We also found that electron-impact excitation of the $6p$ manifold from the $6s$ and $6s'$ levels, though important, could not alone explain the experimental results.

We then investigated heavy-particle quenching of the $5d[3/2]_1$ as the source of the decrease in laser efficiency at high xenon fraction. We parametrized various two- and three-body quenching processes, and found that two-body quenching of the $5d[3/2]_1$ level by atomic xenon is consistent with experimental results. The rate constant we derived for this process is 3×10^{-10} cm^3 s^{-1}. Using this rate constant, calculated laser power efficiency and fractional laser intensities as a function of xenon mole fraction are shown in Figs. 2 and 3. These values are based on total laser energy. The operating conditions are taken from the experiments of Suda *et al.*[6] and Wexler *et al.*[14] for e-beam excitation, and their results are shown in the figures as well. We also show the normalized results of Basov *et al.*,[1] although these results were obtained at somewhat different conditions. The total pressure and power deposition are 4 atm and 42 kW cm^{-3}, and the pulse duration is 2 μs. The decrease in the total laser efficiency and in the fractional laser power at 1.73 μm with increasing xenon mole fraction is largely attributed to the cited quenching by atomic xenon. The increase in the fractional intensity of the 2.63-μm transition is primarily a result of a collisional cascade from the $5d[3/2]_1$ level to the $5d[5/2/]_2$ level. In both experiment and theory the fractional energy at 2.03 μm (not shown) is $<3\%$. The theoretical efficiency maximizes at a slightly lower xenon fraction, indicating that we may be underestimating population of the $6p$ manifold, perhaps by $6s\rightarrow6p$ electron-impact processes. We overestimate the contribution of 2.63 μm because of our lack of oscillation at 2.65 μm, which is observed experimentally. The agreement when including the combined experimental 2.63- and 2.65-μm energies is better.

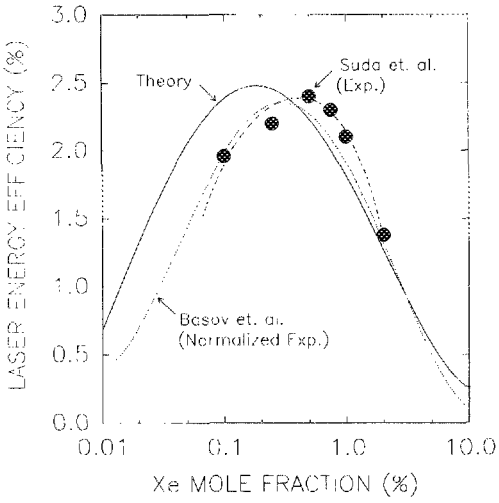

FIG. 2. Laser energy efficiency as a function of xenon mole fraction in an Ar/Xe mixture. The theory uses the conditions of Suda *et al.* (Ref. 6), also shown in the figure, which are a gas pressure of 4 atm, power deposition of 42 kW cm^{-3}, and pulse length of 2 μs. The results of Basov *et al.* (Ref. 1) are also shown for similar conditions.

B. Transient laser spectrum

In spite of the dominance of the 1.73- and 2.63-μm transitions for the optimum conditions described above, laser oscillation is also transiently obtained at 2.03 and 2.65 μm. The transient laser spectrum during multiline oscillation was measured by Suda *et al.*[7] and showed strong competition between the 1.73-, 2.03-, and 2.65-μm transitions, all of which share a common upper laser level. The details of the competition between transitions which have a common upper level depends in large part on the relative magnitude of the quenching coefficients of their lower levels in the $6p$ manifold and of their relative oscillator strengths. For the

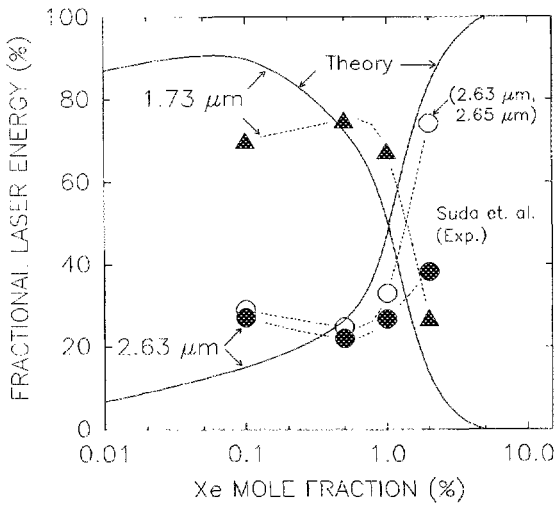

FIG. 3. Theoretical fractional laser energy for the 1.73- and 2.63-μm transitions for the conditions of Suda *et al.* (Ref. 6), also shown in the figure, as described in Fig. 1. The open circles represent the sum of the 2.63- and 2.65-μm transitions.

experimental conditions of Suda *et al.*[7] (4 atm, power deposition 42 kW cm^{-3}), the dominant quenching processes in the $6p$ manifold are collisions with argon. The 2.03- and 2.65-μm transitions are more sensitive to the quenching of their individual lower levels due to the smaller degeneracies of those levels.

The total quenching coefficients for collisions with argon of some levels of the $6p$ manifold have been measured. When using these values, however, we were unable to reproduce the experimentally observed laser spectrum. Although other processes (e.g., electron-impact excitation, dimer formation) contribute to the population and quenching of these lower laser levels, their rates are small compared to quenching by argonunder optimum conditions. Therefore, we chose to parametrize the total quenching rate constants of the three lower levels of these transitions ($6p[5/2]_2$, $6p[3/2]_1$, and $6p[2/1]_0$) within the same order as the measured values while keeping the same branching fractions as those for collisions with xenon. The resulting rate coefficients are in Table III. (The quenching coefficient for $6p[2/1]_0$ is the measured value.)

Calculated time histories of the individual laser lines during multiline oscillation are shown in Fig. 4(a), and the experimental results of Suda *et al.*[7] are shown in Fig. 4(b). The experimental laser energy efficiency is 2.3%, and our calculated value is 2.2%. The time dependencies of the 1.73-, 2.63-, and 2.03-μm transitions are fairly well reproduced.

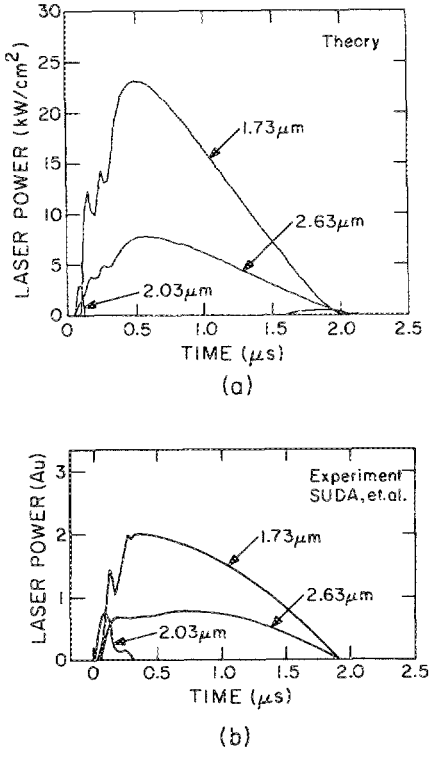

FIG. 4. Xenon laser intensities as a function of time for a gas pressure of 4 atm (Ar/Xe = 99.5/0.5) and average pump rate for 42 kW cm^{-3}. (a) Model results and (b) experimental results of Suda *et al.* (Ref. 7). The relative intensities of the experimental results are approximate. The "ripple" in the 1.73-μm intensity is due to oscillations in the e-beam current. Note the transient oscillation of the 2.03-μm transition at the leading edge of the current pulse.

Oscillation on the 2.03-μm transition occurs during the rise and fall of the current pulse. At these times, the gain is still fairly low, as are the populations of the $6p$ and $6s$ manifolds. As a result, oscillation occurs on the 2.03-μm transition due to its higher oscillator strength compared to the 1.73-μm transition. As the gain increases and the density of the $6p$ manifold increases, the favorable quenching and degeneracy of the lower laser level of the 1.73-μm transition allow it to oscillate with a delay relative to the 2.03-μm transition. At that time the 2.03-μm transition is quenched by saturation of the $5d[3/2]_1$ level. Our results for the 2.65-μm transition are in poor agreement with experiment, which is attributed to a poor representation of the quenching of the $6p[2/1]_0$ level by heavy particles or by electronal collision mixing.

C. The dependence of laser efficiency on gas pressure and power deposition

Since the atomic xenon laser in Ar/Xe mixtures operates most efficiently when the 1.73-μm transition dominates, the optimum operating conditions with respect to gas pressure and power deposition must be ultimately explained in terms of the difference between population and quenching of the $5d[3/2]_1$ level of xenon. In addition to dissociative recombination of $ArXe^+$ and Xe_2^+, which in our model indirectly populate the $5d$ manifold by collisional cascade, and to collisional quenching of xenon excited states by heavy particles, the $6p$ and $5d$ manifolds are also tightly coupled by electron-collision mixing [e.g., $e + Xe(5d[3/2]_1) \rightleftarrows Xe(6p[5/2]_2) + e$]. Electron-collision mixing effectively quenches the $5d$ manifold and populates the $6p$ manifold, driving them towards a thermal distribution characterized by the electron temperature. At sufficiently high rates of electron-collision mixing, laser oscillation will terminate due to this thermalization process.

We examined the importance of electron-collision mixing between the $5d$ and $6p$ manifolds by comparing calculated laser performance to experiments over a wide range of gas pressure and power deposition. The bases of our comparison were measurements of laser power efficiency and laser saturation intensity as a function of gas pressure and power deposition. We found that collisions by excited heavy particles or ions could not explain the observed increase in laser saturation intensity and decrease in laser efficiency, at high-power deposition and constant gas pressure. To do so, their rate constants would have been unphysically large. We hypothesized that electron-collision mixing of the $5d$ and $6p$ manifolds is responsible for the observed behavior. We derived the rate constant for this process by comparing our results with experiments and obtained good agreement with a value of 2×10^{-7} cm^3 s^{-1} for the exothermic process. The rate constants for the endothermic processes are given by detailed balance. (See Sec. IV B.)

Calculated quasi-steady-state intrinsic laser power efficiency as a function of power deposition is shown in Fig. 5 for different gas pressures. The gas mixture is Ar/Xe = 99.5/0.5. The pumping pulse has a rise time of 300 ns, and it then has a constant power deposition at the cited value. The optical cavity consists of a maximum reflector

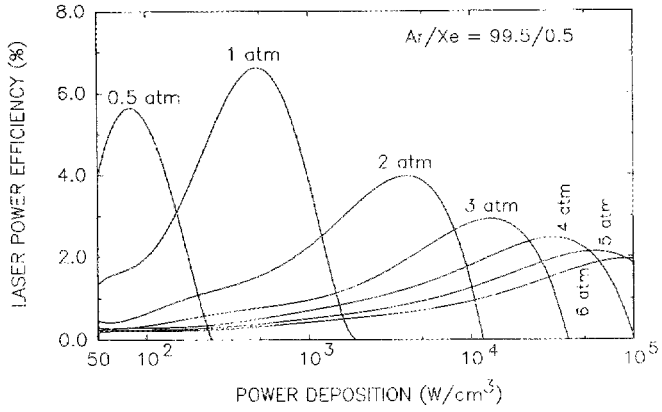

FIG. 5. Intrinsic laser power efficiency (quasi steady state) as a function of e-beam power deposition for different gas pressures. The mixture is Ar/Xe = 99.5/0.5. The rapid decrease in laser efficiency at high pump rate is due to electron-collision mixing of the laser levels.

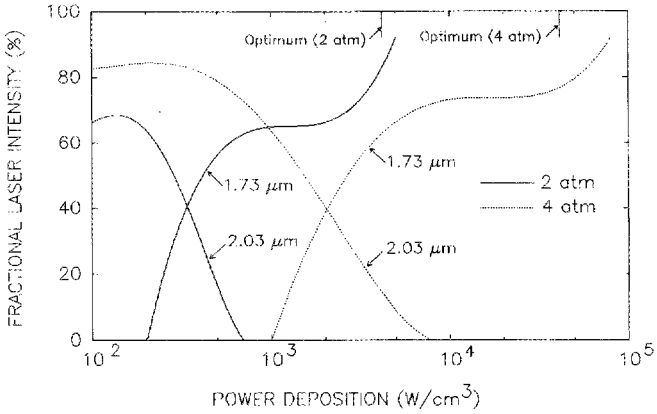

FIG. 7. Fractional laser power for the 1.73- and 2.03-μm transitions as a function of power deposition for Ar/Xe = 99.5/0.5 at 2 and 4 atm. The optimum power depositions are shown for each case. The 1.73-μm transition dominates near and above the optimum power, while the 2.03-μm transition dominates at low-power deposition and gain.

and a 50% reflectivity output mirror separated by 1 m. The same reflectivity was used for all laser transitions. Maximum laser efficiency and plasma parameters for the optimum conditions as a function of gas pressure appear in Fig. 6. Fractional intensities for the laser transitions for the same conditions as Fig. 5 appear in Fig. 7.

The power deposition at which maximum laser efficiency is obtained increases with increasing gas pressure, as shown in Figs. 5 and 6. The maximum intrinsic efficiency for these conditions is obtained at 1 atm with a power deposition of $\approx$250 W cm^{-3}. The maximum laser efficiency decreases at higher gas pressures due to a net increase in quenching of the laser levels by heavy-particle collisions. In spite of the decrease in efficiency with increasing pressure, total laser power increases because the optimum power deposition also increases. (See Fig. 6.) The decrease in laser efficiency at higher power deposition (for a given pressure) is due dominantly to the detrimental effects of electron collision mixing of the $5d$ and $6p$ manifolds. When electron collision mixing begins to dominate, high efficiency is recouped by "bootstrapping" to higher pressure where heavy-particle collisions clear the lower laser level. In most cases, the 1.73-μm transition is the dominant line near the optimum power deposition, regardless of the value of gas pressure over this

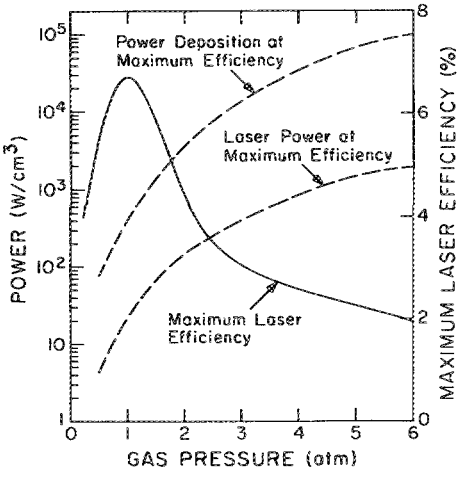

FIG. 6. Intrinsic laser power efficiency at the optimum pump rate as a function of gas pressure for the conditions of Fig. 5. The optimum power deposition and laser power are also shown as a function of pressure. Although laser efficiency decreases with increasing pressure, the total power increases due to the increase in the optimum power deposition.

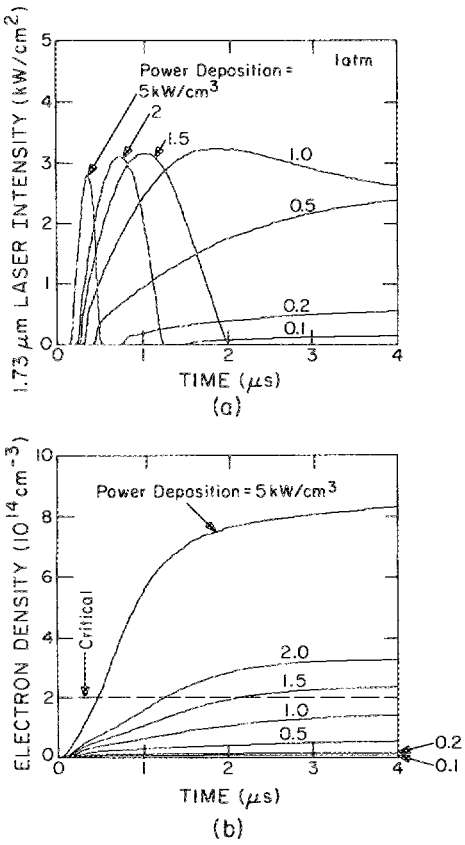

FIG. 8. Laser parameters at power depositions of 100 W cm^{-3} to 5 kW cm^{-3} for a 1-atm Ar/Xe = 99.5/0.5 mixture. (a) Laser intensity at 1.73 μm and (b) electron density. The laser prematurely terminates if the electron density exceeds about 2×10^{14} cm^{-3}, or a fractional ionization of 8×10^{-6}.

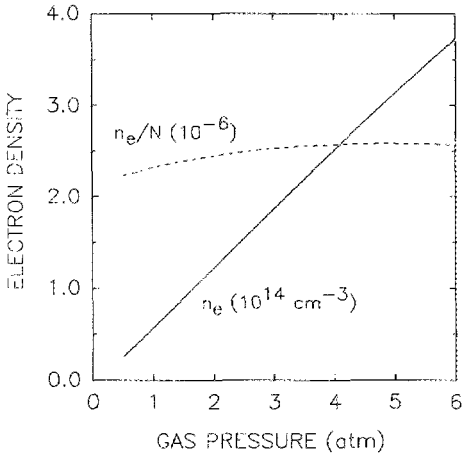

FIG. 9. Electron density and fractional ionization at the optimum pump rate as a function of gas pressure. The conditions are the same as for Fig. 5. Optimum laser efficiency is obtained at a fractional ionization of $2-3\times10^{-6}$.

range of values, as shown in Fig. 7. The exception is that the 2.03-μm transition dominates when the power deposition is much less than the optimum. This occurs because the 2.03-μm transition has a higher oscillator strength that successfully competes with the favorable quenching of the lower level and ratio of degeneracies of the 1.73-μm transition at low-power deposition and low gain. Higher gain conditions therefore preferentially lead to oscillation at 1.73 μm. The dominance of the 1.73-μm transition at higher power deposition may also be attributable to the fact that it is less sensitive to electron collision mixing due to the larger energy separation between its levels. The fractional intensity of the 2.63-μm transition, though, is least sensitive to power deposition, implying that heavy particle collisions are relatively more important to the dynamics of both its upper and lower laser levels.

In order to illustrate the factors that determine the optimum power deposition, time histories of the 1.73-μm transition and electron number density for different power depositions are shown in Fig. 8 for a gas pressure of 1 atm. The time required for the laser output to reach the quasi steady state, if at all, is strongly dependent on the power deposition and electron density. Note that for these conditions the electron density requires 1–2 μs to come to its steady-state values. At low-power deposition, the quenching of the laser levels is dominated by heavy particle collisions, and laser power rapidly comes into equilibrium with the pump rate. At higher power deposition, the electron density increases from below the value at which electron collision mixing dominates to above that value. When this occurs, laser intensity decreases and finally quenches, resulting in premature termination of the laser pulse. The critical electron density for these conditions above which laser oscillation cannot be sustained is $\approx 2\times10^{14}$ cm^{-3} or a fractional ionization of 8×10^{-6}. These results suggest that relative electron number density is the key in determining the laser performance of high-pressure atomic xenon lasers due to the strong coupling between the laser levels by electron-collision mixing. This issue will be discussed in more detail below.

The electron number density and fractional ionization

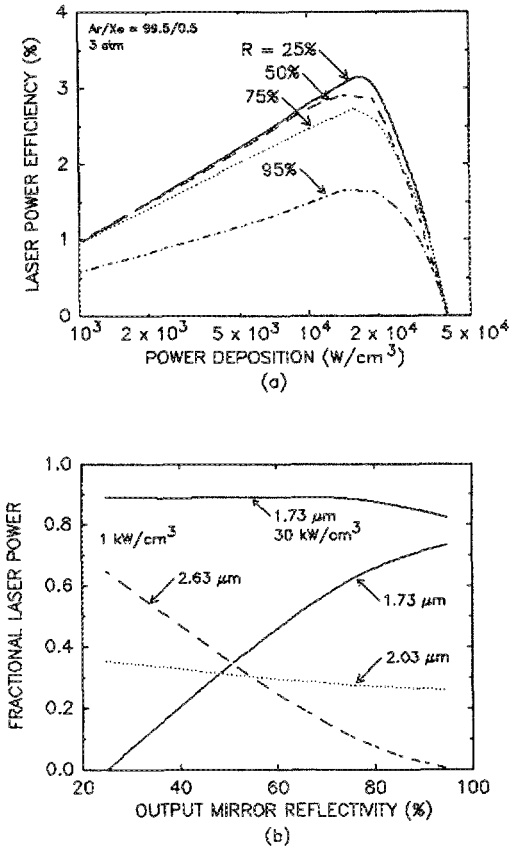

FIG. 10. Laser parameters as a function of out mirror reflectivity. (a) Laser power efficiency as a function of pumping rate for various output mirror reflectivities. The gas pressure is 3 atm (Ar/Xe = 99.5/0.5). Although the maximum efficiency is a function or reflectivity, the power at cutoff has a weak dependence. (b) Laser spectrum as a function of mirror reflectivity at a pump rate of 1 kW cm^{-3}. The fractional laser power at 1.73 μm is also shown for a pump rate of 30 kW cm^{-3}.

as a function of gas pressure at the optimum power deposition are shown in Fig. 9 for the conditions of Fig. 5. The electron number density at optimum deposition increases nearly linearly with increasing gas pressure. The fractional ionization, though, remains approximately constant at $2-3\times10^{-6}$. It appears, then, that it is the fractional ionization which determines the laser performance at high-power deposition in high-pressure atomic xenon lasers; and optimum performance is obtained when the fractional ionization is kept below the value at which electron-collision quenching dominates. These results also suggest that long-duration pumping at moderate power depositions leads to the maximum efficiency with respect to both quasi-steady-state power and specific laser energy.

As one would expect, many of the results presented here are functions of cavity parameters such as mirror reflectivity. For example, oscillation at 1.73 μm can be suppressed by having selective feedback at 2.03 μm as might be obtained when using a grating as the output coupler. In performing such an experiment, Suda *et al.*[6] were able to extend oscillation at 2.03 μm throughout the *e*-beam pulse, as opposed to having it be quenched early during the pulse by oscillation at 1.73 μm (see Fig. 4).

We investigated various aspects of the dependence of laser performance on mirror reflectivity and obtained the

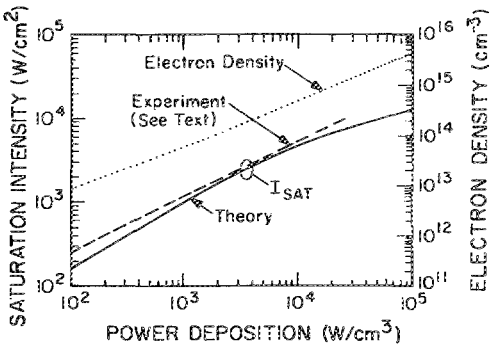

FIG. 11. Experimental and theoretical saturation intensities for the 1.73-μm transition as a function of power deposition. See the text for explanation of the experimental results. The electron density is plotted for reference to show the correlation of saturation intensity with electron density.

results shown in Fig. 10. In Fig. 10(a) laser power efficiency is plotted as a function of power deposition for different mirror reflectivities R. The conditions are Ar/Xe = 99.5/0.5 at 3 atm. The efficiencies are weak functions of R over a fairly wide range. The critical power deposition at termination of oscillation is also at best a weak function of R. The laser spectrum, however, is a strong function of R, at least at low pump power, as shown in Fig. 10(b). At low pump power (1 kW cm^{-3}) the lower gain transitions, such as 1.73 μm, tend to be weak since they are more sensitive to cavity losses. At higher R, the 1.73-μm transition dominates, as it does at higher pump rates where the larger intrinsic gain makes the transition less sensitive to cavity losses.

The experimental validation of the proposal that electron-collision mixing of the $5d$ and $6p$ manifolds largely determines laser performance at high pumping rates is demonstrated by two examples: saturation intensity as a function of pump rate and laser efficiency during long (many ms) pumping pulses. The saturation intensity I_s should increase with increasing gas pressure at low-power deposition because heavy-particle collisions are primarily responsible for determining the lifetimes of the laser levels under those conditions. At higher power deposition electron-collision processes become most important in this regard, and I_s should

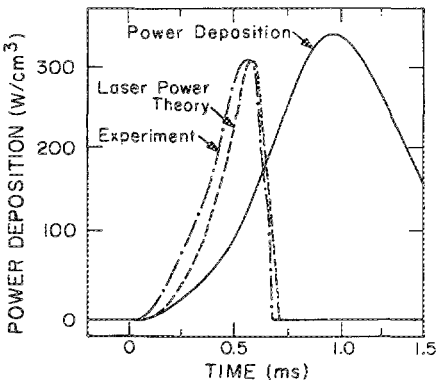

FIG. 12. Laser power and power deposition using fission fragment excitation (0.68 atm, Ar/Xe = 99.5/0.5). The experimental results are those of Alford and Hays (Ref. 9) and the results from the model include the effect of gas heating. The cutoff in laser power is due to the electron density exceeding the critical quenching value.

increase with increasing power deposition. For these conditions, I_s should scale approximately as $P^{0.5}$, which is consistent with the scaling of the electron density in recombination dominated plasmas. In Fig. 11, experimental results for the saturation intensity of the 1.73-μm transition, compiled from many sources,[6,9,14,16,17] are plotted showing this scaling. The calculated values for optimum pumping conditions agree well with the experiments.

The second corroboration can be found with the results of Alford and Hays[9] for fission-fragment excitation of the xenon laser. In their experiment (0.68 atm, Ar/Xe = 99.5/0.5, maximum power deposition = 300 W cm^{-3}), the pumping pulse length is 3–5 ms long and Gaussian in shape. They observed that laser oscillation closely follows the pumping pulse, but then rapidly terminates when a critical power deposition is exceeded, as shown in Fig. 12. Our simulation of their experiment also appears in the figure.[42] Since the pumping pulse is long compared to the kinetic time scale, the electron density is essentially in equilibrium with the power deposition and energy loading. (We have included the effects of gas heating in this calculation, which reduces the rate of recombination and increases the electron density with increasing energy leading.[43]) The rapid termination of laser oscillation is a consequence of the electron density exceeding the value for which electron-collision mixing dominates quenching.

VI. CONCLUDING REMARKS

A model for the electron-beam-excited, high-pressure xenon laser using Ar/Xe mixtures has been presented. Results of the model have been used to investigate the performance of the atomic xenon laser as a function of gas mixture, gas pressure, and power deposition. Our results indicate that the reduction of the laser efficiency at high xenon fractions results primarily from rapid quenching of the upper laser level for the 1.73-μm transition by collisions with xenon. The switching of the dominant line from 1.73 to 2.63 μm at high xenon fraction results from the collisional cascade following this quenching. Laser efficiency was examined over a large parameter space in gas pressure and power deposition. We found that the optimum power deposition shifts to higher values with increasing gas pressure. This scaling suggests that the optimum power deposition for each gas pressure is determined by that value at which electron-collision mixing of the laser levels begins to dominate and to quench laser oscillation. Our results predict that optimum laser efficiency is obtained at the power deposition corresponding to a fractional ionization of $2–3\times10^{-6}$. This suggests that long-duration pumping at moderate power depositions leads to the most efficient extraction of high specific output energy in high-pressure atomic xenon lasers.

ACKNOWLEDGMENTS

The authors wish to thank the following individuals for many stimulating discussions on the topic of this paper and for access to their experimental results prior to publication: G. N. Hays, J. Alford, E. A. Patterson, P. J. Brannon, and D. MacArthur of Sandia National Laboratory; J. Jacob of Science Research Laboratory and B. Wexler of Naval Re-

search Laboratory. We particularly thank J. B. Gerardo of Sandia National Laboratory for pointing out the scaling of laser saturation intensity with power deposition. This work was supported by Sandia National Laboratory.

[1]N. G. Basov, V. V. Baronov, A. Y. Chungunov, V. A. Danilychev, A. Y. Dudin, I. V. Kholin, N. N. Ustinovskii, and D. A. Zayarnyi, IEEE J. Quantum Electron. **QE-21**, 1756 (1985).
[2]N. G. Basov, V. A. Danilychev, A. Yu. Dudin, D. A. Zayarnyl, N. N. Ustinovskii, I. V. Kholin, and A. Yu. Chugunov, Sov. J. Quantum Electron. **14**, 1158 (1984).
[3]G. Basov, A. Yu. Chugunov, V. A. Danilychev, I. V. Kholin, and M. N. Ustinovsky, IEEE J. Quantum Electron. **QE-19**, 126 (1983).
[4]P. J. M. Peters, Q.-C. Mei, and W. J. Witteman, Appl. Phys. B **47**, 187 (1988).
[5]P. J. M. Peters, Q.-C. Mei, and W. J. Witteman, Appl. Phys. Lett. **54**, 193 (1989).
[6]A. Suda, B. L. Wexler, K. Riley, and B. J. Feldmann, IEEE J. Quantum Electron. (to be published).
[7]A. Suda, B. Wexler, B. Feldman, and K. Riley, Appl. Phys. Lett. **54**, 1305 (1989).
[8]V. V. Baranov, V. A. Danilychev, A. Yu. Dudin, D. A. Zayarnyi, N. N. Ustiovskii, I. V. Kholin, and A. Yu. Chugunov, Sov. Phys. Tech. Phys. **11**, 70 (1985).
[9]J. Alford and G. N. Hays, J. Appl. Phys. **65**, 3760 (1989).
[10]C. L. Gordon, B. Feldmann, and C. P. Christensen, Opt. Lett. **13**, 114 (1988).
[11]F. Collier, P. Labastie, M. Maillet, and M. Michon, IEEE J. Quantum Electron. **QE-19**, 1129 (1983).
[12]W. T. Silfvast, L. H. Szeto, and O. R. Wood II, Appl. Phys. Lett. **31**, 223 (1977).
[13]S. A. Lawton, J. B. Richards, L. A. Newman, L. Specht, and T. A. DeTemple, J. Appl. Phys. **50**, 3888 (1979).
[14]B. L. Wexler, A. Suda, J. E. Tucker, B. J. Feldman, and K. Riley, in Technical Digest of the Conference on Lasers and Electrooptics, Anaheim, CA, April 1988, paper WP3.
[15]J. E. Tucker, B. L. Wexler, B. Feldman, and T. McClelland, Photon. Technol. Lett. **1**, 193 (1989).
[16]J. Jacob, Science Research Laboratories (private communication, 1988).
[17]E. L. Patterson, G. E. Samlin, and P. J. Brannon, in Technical Digest of the Conference on Lasers and Electro-Optics, Baltimore, MD, April 1989, paper WF21.
[18]Y.-J. Shiu, M. A. Biondi, and D. W. Sipler, Phys. Rev. A **15**, 494 (1977).
[19]Y.-J. Shiu and M. A. Biondi, Phys. Rev. A **17**, 868 (1978).
[20]J. K. Ku and D. W. Setser, J. Chem. Phys. **84**, 4304 (1986).
[21]F. Kannari, A. Suda, M. Obara, and T. Fujioka, IEEE J. Quantum Electron. **QE-19**, 1587 (1983).
[22]H. Hokazono, K. Midorikawa, M. Obara, and T. Fujioka, J. Appl. Phys. **56**, 680 (1984).
[23]F. Kannari, M. Obara, and T. Fujioka, J. Appl. Phys. **57**, 4307 (1985).
[24]M. J. Kushner, J. Appl. Phys. **66**, 2297 (1989).
[25]J. N. Bardsley and M. A. Biondi, Adv. At. Mol. Phys. **6**, 2 (1970); J. Boker and C. K. Rhodes, J. Chem. Phys. **73**, 2626 (1980).
[26]T. F. O'Malley, Phys. Rev. **185**, 101 (1969).
[27]L. G. Piper, J. E. Velazco, and D. W. Setser, J. Chem. Phys. **59**, 3323 (1973).
[28]J. H. Kolts and D. W. Setser, in Proceedings of the 7th Winter Colloquium on High Power Visible Lasers, Park City, Utah, 1977.
[29]C. A. Brau, in *Excimer Lasers*, edited by C. K. Rhodes (Springer, Berlin, 1979), pp. 87–134.
[30]R. E. Gleason, T. D. Bonifield, J. W. Keto, and G. K. Walters, J. Chem. Phys. **66**, 1589 (1977).
[31]L. Allen, D. G. C. Jones, and D. G. Schofield, J. Opt. Soc. Am. **59**, 842 (1969).
[32]D. C. Lorents, D. J. Eckstrom, and D. Huestis, Stanford Research Institute Report MP73-2, September 1973.
[33]J. K. Rice and A. W. Johnson, J. Chem. Phys. **63**, 5235 (1975).
[34]H. Horiguchi, R. S. F. Chang, and D. W. Setser, J. Chem. Phys. **75**, 1207 (1981).
[35]N. Bowering, M. R. Bruce, and J. W. Keto, J. Chem. Phys. **84**, 709 (1986).
[36]G. Inoue, J. K. Ku, and D. W. Setser, J. Chem. Phys. **81**, 5760 (1984).
[37]M. Aymar and M. Coulombe, At. Data Nucl. Data Tables **21**, 537 (1978).
[38]D. L. King, L. G. Piper, and D. W. Setser, J. Chem. Soc. Faraday Trans. II **73**, 177 (1977).
[39]M. Krause and F. H. Mies, in *Excimer Lasers*, edited by Ch. K. Rhodes (Springer, New York, 1984).
[40]L. A. Levin, S. E. Moody, E. L. Klosterman, R. E. Center, and J. J. Ewing, IEEE J. Quantum Electron. **QE-17**, 2282 (1981).
[41]T. Holstein, Phys. Rev. **72**, 1212 (1947); Phys. Rev. **83**, 1159 (1951).
[42]We have previously shown that for these conditions fission-fragment excitation and *e*-beam excitation may be compared on the basis of power deposition to an accuracy of 10%–15%. See T. J. Moratz, T. D. Saunders, and M. J. Kushner, J. Appl. Phys. **64**, 3799 (1988).
[43]T. J. Moratz, T. D. Saunders, and M. J. Kushner, Appl. Phys. Lett. **54**, 102 (1989).